

# Locality-Sensitive Hashing for Earthquake Detection: A Case Study Scaling Data-Driven Science

Kexin Rong\*, Clara E. Yoon<sup>†</sup>, Karianne J. Bergen<sup>‡</sup>, Hashem Elezabi\*,  
Peter Bailis\*, Philip Levis\*, Gregory C. Beroza<sup>†</sup>  
Stanford University

## ABSTRACT

In this work, we report on a novel application of Locality Sensitive Hashing (LSH) to seismic data at scale. Based on the high waveform similarity between reoccurring earthquakes, our application identifies potential earthquakes by searching for similar time series segments via LSH. However, a straightforward implementation of this LSH-enabled application has difficulty scaling beyond 3 months of continuous time series data measured at a single seismic station. As a case study of a data-driven science workflow, we illustrate how domain knowledge can be incorporated into the workload to improve both the efficiency and result quality. We describe several end-to-end optimizations of the analysis pipeline from pre-processing to post-processing, which allow the application to scale to time series data measured at multiple seismic stations. Our optimizations enable an over 100 $\times$  speed up in the end-to-end analysis pipeline. This improved scalability enabled seismologists to perform seismic analysis on more than ten years of continuous time series data from over ten seismic stations, and has directly enabled the discovery of 597 new earthquakes near the Diablo Canyon nuclear power plant in California and 6123 new earthquakes in New Zealand.

## 1 INTRODUCTION

Locality Sensitive Hashing (LSH) [27] is a well studied computational primitive for efficient nearest neighbor search in high-dimensional spaces. LSH hashes items into low-dimensional spaces such that similar but not exact items are placed in the same hash table bucket with higher probability. Successful applications of LSH include entity resolution [58], genome sequence comparison [16], text and image search [38, 48], near duplicate detection [18, 43], and video identification [34].

In this paper, we present an innovative use of LSH—and associated challenges at scale—in large-scale earthquake detection across seismic networks. Earthquake detection is particularly interesting in both its abundance of raw data and scarcity of labeled examples:

First, seismic data is large. Earthquakes are monitored by seismic networks, which can contain thousands of seismometers that continuously measure ground motion and vibration. For example, Southern California alone has over 500 seismic stations, each collecting continuous ground motion measurements at 100Hz. As a result, the network has collected over ten trillion ( $10^{13}$ ) data points in the form of time series in the past decade alone [5].

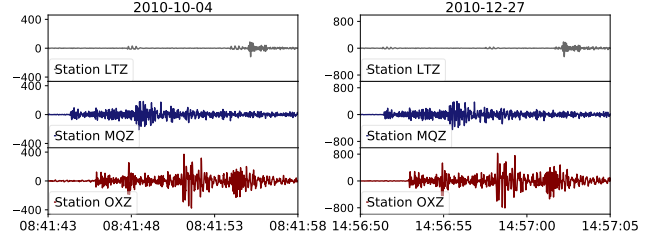


**Figure 1: Example of the near identical waveforms between two occurrences of the same earthquake two months apart, observed at three seismic stations in New Zealand. This paper scales LSH to over 30 billion data points, which results in the discoveries of 597 new earthquakes near the Diablo Canyon nuclear power plant in California as well as 6123 new local earthquakes in New Zealand.**

Second, despite large measurement volumes, only a small fraction of earthquake events are cataloged, or confirmed and hand-labeled. As earthquake magnitude (i.e., size) decreases, the frequency of earthquake events increases exponentially. Worldwide, major earthquakes (magnitude 7+) occur approximately once a month, while magnitude 2.0 and smaller earthquakes occur several thousand times a day. At low magnitudes, it is difficult to detect earthquake signals because earthquake energy approaches the noise floor, and conventional seismological analyses can fail to disambiguate between signal and noise. Nevertheless, detecting these small earthquakes is important in uncovering sources of earthquakes [22, 29], improving the understanding of earthquake mechanics [45, 53], and better predicting future events [35].

To take advantage of the large volume of unlabeled raw measurement data, seismologists have developed an unsupervised, data-driven earthquake detection method, Fingerprint And Similarity Thresholding (FAST), based on waveform similarity [23]. Specifically, seismic sources repeatedly generate earthquakes over the course of days, months or even years, and these earthquakes show near identical waveforms when recorded at the same seismic station, regardless of the earthquake’s magnitude [25, 51]. Figure 1 illustrates this phenomenon by depicting two similar earthquakes that are two months apart, observed at three seismic stations in New Zealand. By applying LSH to identify similar waveforms from seismic data, seismologists were able to discover new, low-magnitude earthquakes without knowledge of prior earthquake events.

However, despite early success, seismologists had difficulty scaling their LSH-based analysis beyond 3-month of time series data

\* Department of Computer Science.

<sup>†</sup> Department of Geophysics.

<sup>‡</sup> Institute for Computational and Mathematical Engineering.

( $7.95 \times 10^8$  data points) at a single seismic station [22]. The FAST implementation faces severe scalability challenges. Contrary to what LSH theory suggests, the actual LSH runtime in FAST grows near quadratically with the input size due to correlations in the seismic signals: in an initial performance benchmark, the similarity search took 5 CPU-days to process 3 months of data, and, with a  $5\times$  increase in dataset size, LSH query time increased by  $30\times$ . In addition, station-specific repeated background noise leads to an overwhelming number of similar but non-earthquake time series matches, both crippling throughput and seismologists’ ability to sift through the output, which can number in the hundreds of millions of events. Ultimately, these scalability bottlenecks prevented seismologists from making use of the decades of data at their disposal.

In this paper, we show how systems, algorithms, and domain expertise can go hand-in-hand to deliver substantial scalability improvements for this seismological analysis. Via algorithmic design, optimization using domain knowledge, and data engineering, we scale the FAST workload to years of continuous data at multiple stations. In turn, this scalability has enabled new scientific discoveries, including previously unknown earthquakes near a nuclear reactor in San Luis Obispo, California, and in New Zealand.

Specifically, we build a scalable end-to-end earthquake detection pipeline comprised of three main steps. First, the fingerprint extraction step encodes time-frequency features of the original time series into compact binary fingerprints that are more robust to small variations and noise. To address the bottleneck caused by repeating non-seismic signals, we apply domain-specific filters based on the frequency range of seismic waves and the frequency of earthquake occurrence. Second, the search step identifies all pairs of similar time series segments by performing a similarity search on the binary fingerprints via LSH. We pinpoint high hash collision rates caused by physical correlations in the input data as a core culprit of LSH performance degradation and alleviate the impact of large buckets by increasing hash selectivity while keeping the detection threshold constant. Third, to reduce output size, the alignment step aggregates detection results and confirms seismic behavior by performing spatiotemporal correlation with nearby seismic stations in the network [13]. To scale this analysis, we leverage domain knowledge of the invariance of the time difference between a pair of earthquake events across all stations at which they are recorded.

In summary, as an innovative systems and applications paper, this work makes several contributions:

- We report on a new application of LSH in seismology as well as a complete end-to-end data science pipeline, including non-trivial pre-processing and post-processing, that scales to a decade of continuous time series for earthquake detection.
- We present a case study for using domain knowledge to improve the accuracy and efficiency of the pipeline. We illustrate how applying seismological domain knowledge in each component of the pipeline is critical to scalability.
- We demonstrate that our optimizations enable a cumulative two order-of-magnitude speedup in the end-to-end detection pipeline. These quantitative improvements enable qualitative discoveries: we discovered 597 new earthquakes near the Diablo Canyon nuclear power plant in California and 6123

new earthquakes in New Zealand, allowing seismologists to determine the size and shape of nearby fault structures.

Beyond these contributions to a database audience, our solution is an open source tool, available for use by the broader scientific community. We have already run workshops for seismologists at Stanford [2] and believe that the pipeline can not only facilitate targeted seismic analysis but also contribute to the label generation for supervised methods in seismic data [46].

The rest of the paper proceeds as follows. We review background information about earthquake detection in Section 2 and discuss additional related work in Section 3. We give a brief overview of the end-to-end detection pipeline and key technical challenges in Section 4. Sections 5, 6 and 7 present details as well as optimizations in the fingerprint extraction, similarity search and the spatiotemporal alignment steps of the pipeline. We perform a detailed evaluation on both the quantitative performance improvements of our optimizations as well as qualitative results of new seismic findings in Section 8. In Section 9, we reflect on lessons learned and conclude.

## 2 BACKGROUND

With the deployment of denser and increasingly sensitive sensor arrays, seismology is experiencing rapid growth of high-resolution data [28]. Seismic networks consisting of up to thousands of sensors record years of continuous seismic data streams, typically at 100Hz frequencies. This massive volume of data has fueled strong interest in the seismology community to apply and develop scalable algorithms that automate and improve the monitoring and prediction of earthquake events [19, 37, 39].

In this work, we focus on the problem of detecting new, low-magnitude earthquakes from historical seismic data. Earthquakes, which are primarily caused by the rupture of geological faults, radiate energy that travels through the Earth in the form of seismic waves. Seismic waves induce ground motion that is recorded by seismometers. Modern seismometers typically include 3 components that measure simultaneous ground motion along the north-south, east-west, and vertical axes. Each direction of movement, often referred to as a *channel*, contains information about the earthquake.

These low-magnitude earthquakes pose a challenge for conventional methods for detection, which we outline below. Almost all earthquakes greater than magnitude 5 are detected [24]. However, an estimated 1.5 million earthquakes with magnitude between 2 and 5 are not detected by conventional means, and 1.3 million of these are between magnitude 2 and 2.9. We are interested in detecting these low-magnitude earthquakes missing from public earthquake catalogs to better understand earthquake mechanics and sources, which inform seismic hazard estimates and prediction [29, 35, 45, 53].

Traditional energy-based earthquake detectors such as a short-term average (STA)/long-term average (LTA) identify earthquake events by their impulsive, high signal-to-noise seismic waves (i.e., ratio of P-wave and S-wave arrival). However, these detectors are prone to high false positive and false negative rates at low magnitudes, especially with noisy backgrounds and/or weak signals as in a station that is distant from a low magnitude event [26]. Template matching, or the waveform cross-correlation with template waveforms of known earthquakes, has proven more effective for

detecting known seismic signals in noisy data [14, 52]. However, the template matching relies on template waveforms of prior events and is not suitable for discovering events from unknown sources.

The earthquake detection pipeline we study in the paper is an unsupervised and data-driven approach that does not rely on supervised (i.e., labeled) examples of prior earthquake events, and is designed to complement existing, supervised detection methods. As in template matching, the method we optimize takes advantage of the high similarity between waveforms generated by reoccurring earthquakes. However, instead of relying on waveform templates from known events, the pipeline leverages the recurring nature of seismic activity to detect similar waveforms in time and across stations. To do so, the pipeline performs an all-pair time series similarity search, treating each segment of the input waveform data as a “template” for potential earthquakes. This pipeline will not detect an earthquake that occurs only once and is not similar enough to any other earthquakes in the input data, so, to improve detection recall, it is critical to be able to scale the analysis to input data with longer duration (e.g., years instead of weeks or months).

### 3 RELATED WORK

In this section, we address related work in earthquake detection, LSH-based applications and time series similarity search.

**Earthquake Detection.** The original FAST work appeared in the seismology community, and has proven a useful tool in scientific discovery [22, 23]. In this paper, we present FAST to a database audience for the first time, and report on both the pipeline composition and optimization from a computational perspective. The results presented in this paper are the result of over a year of collaboration between our database research group and the Stanford earthquake seismology research group. The optimizations we present in this paper and the resulting scalability results of the optimized pipeline have not previously been published. We believe this represents a useful and innovative application of LSH to a real domain science tool that will be of interest to both the database community and researchers of LSH and time-series analytics.

The problem of earthquake detection is decades-old [6], and many classic techniques—many of which are in use today—were developed for an era in which humans manually inspected seismographs for readings [32, 59]. With the rise of machine learning and large-scale data analytics, there has been increasing interest in further automating these techniques. While FAST is optimized to find many small-scale earthquakes, alternative approaches in the seismology community utilize template matching [14, 52], social media [50], and machine learning including neural networks [8, 57]. Most recently, with sufficient training data, supervised approaches such as [46] have the advantage of being able to detect non repeating earthquake events. In contrast, our LSH-based detection method is unsupervised, and therefore does not rely on labeled earthquake events. In the evaluation, we show that this unsupervised method is able to detect 597 new earthquakes, with 355 new earthquakes in the particular area of interest, despite the low overall earthquake activity (535 cataloged events over 10 years) in the area of interest.

**Locality Sensitive Hashing.** In this work, we perform a detailed case study of the practical challenges of applying LSH to the domain of seismology and propose domain-specific solutions to address

these challenges. We do not contribute to the advance of the state-of-the-art LSH algorithms. Instead, we show that classic LSH techniques, with domain-specific optimizations, can lead to scientific discoveries, while posing substantial computational challenges at scale. Existing work shows that LSH performance is sensitive to key parameters such as number of hashes [21, 49]; we provide supporting evidence and detailed analysis on the performance implication of LSH parameters in our application domain. In addition to the core LSH techniques, we also present nontrivial preprocessing and postprocessing steps that enable an end-to-end detection pipeline, including spatiotemporal alignment of LSH matches.

While there are exciting opportunities to significantly speed up the similarity search on GPUs [31], this work focuses on CPU workloads. To preserve the integrity of the established workflow, instead of replacing the MinHash based LSH with potentially more efficient LSH variants such as LSH forest [10] and multi-probe LSH [42], we focus on optimizing an existing implementation of Minhash LSH for the application domain. We also provide performance benchmarks against, FALCONN, an open source LSH library based on recent theoretical advances in LSH for cosine similarity. We believe the resulting experience report—and several key challenges we encountered including fingerprint non-uniformity and repeated noise—as well as our open source implementation will be valuable to researchers developing LSH techniques in the future.

**Time Series Analytics.** Time series analytics is a core topic in large-scale data analytics and data mining [36, 41]. In our application domain, we utilize time series similarity search as a core workhorse in earthquake detection. There are a range of computational primitives that could be applied to this problem [20], including Euclidean distance and its variants [60], Dynamic Time Warping [47], and edit distance [56]. However, the input time series coming from seismometer measurements to our application is high frequency (e.g. 100Hz) and potentially noisy. Therefore, small time-shifts, outliers and scaling can result in large changes in time-domain metrics [17].

Instead, we encode time-frequency features of the input time series into binary vectors and focus on the Jaccard similarity. This feature extraction procedure is an adaptation of the Waveprint algorithm [9] originally designed for audio data; the key modification made for seismic data was to focus on frequency features that are the most discriminative from background noise, such that the average similarity between non-seismic signals are reduced [12]. An alternative binary representation models time series as points on a grid, and uses the non-empty grid cells as a set representation of the time series [44]. However, this representation does not take advantage of the physical properties distinguishing background from seismic signals.

### 4 PIPELINE OVERVIEW

In this section, we provide an overview of our unsupervised detection pipeline from feature extraction to post-processing. We provide a detailed description of each step in the pipeline—and our associated optimizations—in later sections, referenced inline.

The input of the detection pipeline consists of continuous ground motion measurements in the form of time series, collected from multiple stations in the seismic network. The output of the pipeline

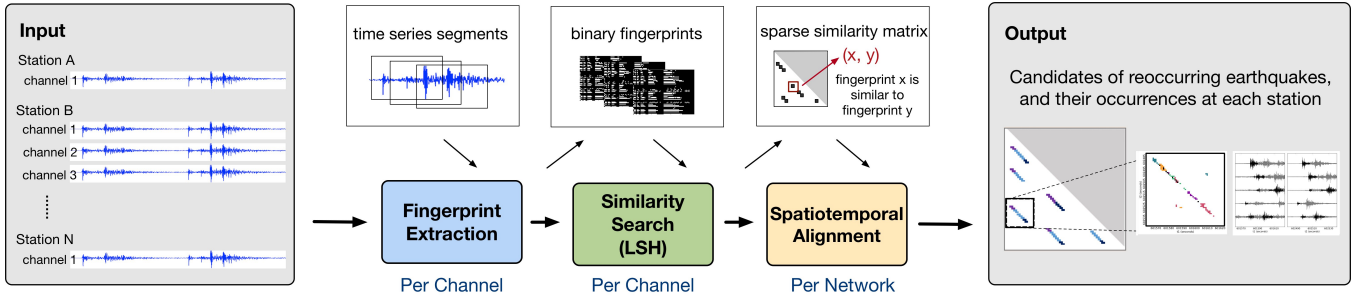


**Figure 2: The three steps of the end-to-end earthquake detection pipeline: fingerprinting transforms time series into binary vectors (Section 5); similarity search identifies pairs of similar binary vectors (Section 6); alignment aggregates and reduces false positives in results (Section 7).**

is a list of potential earthquakes, specified in the form of timestamps when the seismic wave arrives at each station. From there, seismologists can compare timestamps with public earthquake catalogs to identify new events, and visually inspect the measurements to confirm seismic findings.

Figure 2 gives an overview of the end-to-end detection pipeline, which includes three main steps: fingerprint extraction, similarity search, and spatiotemporal alignment. For each input time series, or continuous ground motion measurements from a seismic channel, the algorithm slices the input into short windows of overlapping time series segments and encodes time-frequency features of each window into a binary fingerprint; the similarity of the fingerprints resembles that of the original waveforms (Section 5). The algorithm then identifies pairs of highly similar fingerprints through an all pairs similarity search implemented via LSH (Section 6). The similarity search outputs a sparse similarity matrix for each input time series, where the non-zero entries of the matrix represent similar pairs of fingerprints. Like a traditional associator that maps earthquake detections at each station to a consistent seismic source, in the spatiotemporal alignment stage, the algorithm combines, filters and clusters the outputs from all seismic channels to generate a list of candidate earthquake detections with high confidence (Section 7).

A naïve implementation of the pipeline imposes serious scalability challenges. For example, we observed a degradation of LSH performance in our application domain caused by the non-uniformity and correlation in the binary fingerprints; the correlations induce undesired LSH hash collisions, which significantly increase the number of lookups per similarity search query (Section 6.3). The similarity search does not distinguish seismic from non-seismic signals. In the presence of repeating background signals, similar noise waveforms could outnumber similar earthquake waveforms, leading to more than an order of magnitude slow down in runtime and increase in output size (Section 6.5). As the input time series and the output of the similarity search becomes larger, the pipeline must adapt to data sizes that are too large to fit into main memory (Section 6.4, 7.2).

In this paper, we focus on single-machine, main-memory execution on commodity servers and multicore processors. We parallelize the pipeline within a given server but otherwise do not distribute

the computation to multiple servers. In principle, the parallelization efforts extend to distributed execution. However, given the poor quadratic scalability of the unoptimized pipeline, distribution would not have been a viable option for scaling to our target of a decade of data. As a result of the optimizations described in this paper, we are able to scale to decades of data on a single node without requiring distribution. However, we view distributed execution as worthwhile extension for future work.

In the remaining sections of this paper, we describe the design decisions as well as performance optimizations for each pipeline component. Most of our optimizations focus on the all pairs similarity search, where our initial implementation exhibited near quadratic growth in runtime with the input size. We show in the evaluation that, these optimizations enable speedups of more than two orders of magnitude in the end-to-end detection pipeline.

## 5 FINGERPRINT EXTRACTION

In this section, we describe the fingerprint extraction step that encodes the time-frequency features of the input time series into compact binary vectors for similarity search. We begin with an overview of the fingerprinting algorithm and discuss the benefits of using fingerprints in place of the time series (Section 5.1). We then describe an optimization that accelerates the fingerprinting generation via sampling (Section 5.2).

### 5.1 Fingerprint Overview

The fingerprinting step transforms the continuous time series data into compact binary vectors (fingerprints) for similarity search. The fingerprints are compact encoding of the time-frequency features of the time series data. The Jaccard similarity between binary fingerprints, defined as the size of the intersection of the non-zero entries divided by the size of the union, approximates the pairwise waveform similarity of the original time series segments.

Similar fingerprinting techniques have already seen a successful application on audio signals [9]. Compared to directly computing similarity on the time series, fingerprinting has three main advantages. First, fingerprints extract information about representative frequencies of the input signal, a feature commonly used in earthquake detection. By focusing on the most discriminative frequencies, the fingerprints provide additional robustness to small



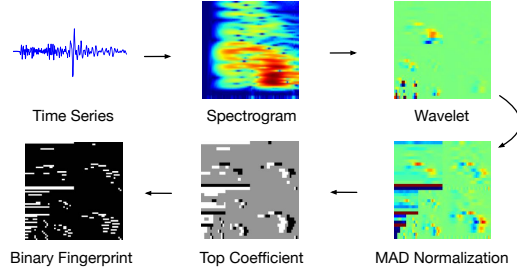


**Figure 3: The fingerprinting algorithm encodes time-frequency features of the time series into binary vectors.**

variations and additive noise and empirically improves detection accuracy [12]. Second, while small time shifts can cause large differences in time-domain similarity metrics such as Euclidean distances, the spectrogram content varies more slowly with time. As a result, we can find similar segments of seismic signals using fewer sliding windows on the spectrogram (e.g., 1-second lag) compared to on the time series (e.g. 0.1-second lag), which reduces the input size for the similarity search. Finally, since each fingerprint only keeps information about a small set of representative features, the resulting sparsity of the binary vector makes it amenable to further efficient dimensionality reduction techniques such as LSH.

Figure 3 illustrates the individual steps for fingerprinting:

- (1) **Spectrogram** Compute the spectrogram, a time-frequency representation, of the time series data. Slice the spectrogram it into short overlapping segments using a sliding window and smooth by downsampling each segment into a spectral image of fixed dimensions.
- (2) **Wavelet Transform** Compute two-dimensional discrete Haar wavelet transform on each spectral image. The wavelet coefficients are a lossy compression of the spectral images.
- (3) **Normalization** Normalize each wavelet coefficient by its median and the median absolute deviation (MAD) on the full, background dominated dataset.
- (4) **Top coefficient** Extract the top  $K$  most anomalous wavelet coefficients, or the largest coefficients after MAD<sup>1</sup> normalization, from each spectral image. By selecting the most anomalous coefficients, we focus only on coefficients that are most distinct from coefficients that characterize noise, which empirically leads to better detection results.
- (5) **Binarize** Binarize the signs and positions of the top wavelet coefficients. Concretely, we encode the sign of each normalized coefficient using 2 bits:  $-1 \rightarrow 01$ ,  $0 \rightarrow 00$ ,  $1 \rightarrow 10$ .

## 5.2 Optimization: MAD via sampling

The fingerprint extraction is implemented via scientific modules such as scipy, numpy and PyWavelets in Python. While its runtime grows linearly with input size, it can take several days to fingerprint ten years of time series data.

In the unoptimized procedure, normalizing the wavelet coefficients requires two full passes on the data. In the first pass, we calculate the median and the MAD for each coefficient across the

<sup>1</sup>For  $X = \{x_1, x_2, \dots, x_n\}$ , the MAD is defined as the median of the absolute deviations from the median:  $MAD = \text{median}(|x_i - \text{median}(X)|)$

whole population, and in the second pass, we normalize the wavelet representations of each fingerprint accordingly.

Given the median and MAD for each wavelet coefficient, we can instead divide the input time series into partitions and normalize them in parallel. Therefore, the calculation of the median and MAD remains the runtime bottleneck.

We accelerate the median and MAD calculation by sampling a small portion of the input data to approximate the true median and MAD. We randomly sample a continuous segment representing  $X\%$  of the time series for each fixed interval (e.g. 1% every hour), and compute the median and the MAD from the sampled data.

The confidence interval for MAD with a sample size of  $n$  shrinks with  $n^{1/2}$  [54]. In the evaluation, we investigate the trade-off between speed and accuracy for different sampling rates (Section 8.3). We empirically find that, on one month of input time series data, sampling provides an order of magnitude speedup with almost no loss in accuracy. For input time series of longer duration, sampling 1% or less of the input can suffice.

## 6 LSH-BASED SIMILARITY SEARCH

In this section, we present the pipeline’s time series similarity search, based on LSH. We begin with a description of the baseline implementation of the similarity search (Section 6.1). We subsequently describe and address a runtime bottleneck in the hash signature generation caused by cache locality (Section 6.2), and a bottleneck in the search caused by large hash collisions (Section 6.3). We further reduce the runtime and memory usage of the search by partitioning and parallelizing (Section 6.4). Finally, we show how domain knowledge of the frequency range and the frequency of occurrences of the earthquakes can significantly speed up the search in the presence of persistent background noise (Section 6.5).

### 6.1 Prior Implementation

Reoccurring earthquakes generated from nearby seismic sources show near-identical waveforms at the same seismic station. Given continuous ground motion measurements from a seismic station, we utilize similarity search to identify all pairs of time series segments that are above a similarity threshold as candidate earthquake events.

To identify pairs of similar time series segments, we perform an approximate nearest neighbor search and identify pairs of binary fingerprints whose Jaccard similarity exceeds a predefined threshold using MinHash LSH [15]. Intuitively, MinHash LSH performs a random projection of high-dimensional data into lower dimensional space, hashing similar items in the low dimensional space to the same hash table “bucket” with high probability. Instead of performing the naïve  $n^2$  comparisons between all pairs of fingerprints, we need only compare fingerprints that share a hash bucket, significantly reducing the number of comparisons required. We refer to the ratio of average comparisons per query to the size of the dataset as *selectivity*, a machine-independent proxy for efficiency [21].

**Hash signature generation.** The MinHash value of a fingerprint is defined as the first non-zero element of the fingerprint under a given random permutation of fingerprint elements. Given  $k$  hash functions, we generate  $k$  independent hash mappings per hash table. Hash function  $h_i(j)$  gives the order of the  $j^{\text{th}}$  element in the fingerprint in the  $i^{\text{th}}$  hash mapping. For each fingerprint and each

hash mapping  $i$ , the minimum hash value is computed among all nonzero elements in the fingerprint. The number of hash functions  $k$  decreases the collision probability by combining every  $k$  MinHash values into a single hash signature. For example, if  $p$  is the probability that one MinHash value declares a pair of fingerprints to be near neighbor candidates, combining  $k$  values lowers the probability to  $p^k$  ([40] provides an overview). In sum, the hash signature generation step computes one hash signature for each fingerprint in each hash table.

**Hash table construction.** We initialize each hash table with its corresponding set of hash signatures. The hash tables map each hash signature to a list of fingerprints that share the same signature. Empirically, we find that using  $t = 100$  hash tables suffices for our application, and there is little gain in further increasing the number of hash tables.

**Search.** The similarity search queries the hash tables for each fingerprint’s candidate near neighbors. Each hash table looks up the query fingerprint  $q$ ’s hash signature and retrieves the corresponding hash bucket. For all other fingerprints  $p_1, \dots, p_n$  in the same hash bucket, we increment the count for  $p_i$  in a map that tracks of the number of times the query fingerprint  $q$  share the hash signature with other fingerprints. After checking all hash tables, the search outputs all fingerprints in the tracking map that have counts over the number of matches threshold. The counts for the number of matches are also included in the output as a proxy for the confidence of the similarity for the final step of the pipeline.

## 6.2 Optimization: Hash signature generation

In this subsection, we present both memory access pattern and algorithmic improvements to speed up the generation of hash signatures. We show that, together, the optimizations can lead to an over  $3\times$  improvement in hash generation time (Section 8.1).

**Cache Locality.** A naive implementation of the MinHash generation suffers from poor memory locality for sparse data. The MinHash is only calculated over the hash values for non-zero elements in the fingerprint, and each fingerprint has few non-zero entries. Therefore, the innermost loop that calculates the MinHash value for each fingerprint performs many random access to the array that stores all hash mappings, leading to an increase in cache misses. As a result, the hash generation runtime is bottlenecked on loading and evicting parts of the hash mapping array to and from cache. We improve the memory access pattern by blocking the access to the MinHash hash table. Rather than iterating by hash function in the inner loop of MinHash (which incurs the above cache misses), we iterate by fingerprint, calculating its MinHash values for all hash functions simultaneously. The  $i$ th entry for each hash function is stored contiguously in memory, incurring an expected one cache miss per fingerprint instead of one per fingerprint and hash function.

**Min-max hash.** We further speed up the hash signature generation by replacing MinHash with Min-Max hash. In MinHash, only the minimum hash value is kept for each random hash mapping. Min-Max hash, on the other hand, keep both the min and the max value which means that it generates two hashes from each hash mapping. Therefore, to generate hash signatures of the same length,

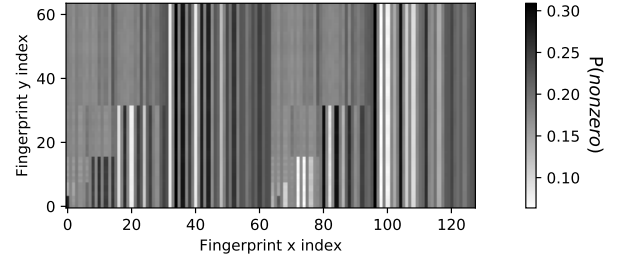


**Figure 4: Probability that each element in the fingerprint is equal to 1, averaged over 15.7M fingerprints, each of dimension 8192, generated from a year of time series data. The heatmap shows that some elements of the fingerprint are much more likely to be non-zero compared to others.**

Min-Max hash reduces the number of required hash mappings to half. Previous work showed the Min-Max hash is an unbiased estimator of pairwise Jaccard similarity, and achieves similar and sometimes smaller mean squared error (MSE) in estimating pairwise Jaccard similarity in practice [30].

## 6.3 Optimization: Alleviating hash collisions

Perhaps surprisingly, our initial LSH implementation demonstrated poor scaling with the input size: with a  $5\times$  increase in put size, the runtime increased by  $30\times$ . In this subsection, we analyze the cause of LSH performance degradation and the performance implications of core LSH parameters in our application.

**Cause of hash collisions.** Poor distribution of hash signatures can lead to large LSH hash buckets and high query *selectivity*, significantly degrading the performance of LSH queries [10, 33]. For example, in the extreme case when the hash table contains a single hash bucket, the *selectivity* equals 1 and the LSH performance is equivalent to that of the naive  $O(n^2)$  all pairs search.

We found that the large hash buckets reflect physical correlations in the data. Elements of the binary fingerprints encode physical properties of the waveform data, so the probability that each element in the fingerprint is non-zero is not uniform (Figure 4). Moreover, elements of the fingerprints are not guaranteed to be independent, meaning that the probability that two elements  $a_i, a_j$  both equal 1 can be much larger than the product of the probability that each element equals 1 ( $\mathbb{P}[a_i = 1, a_j = 1] > \mathbb{P}[a_i = 1] \times \mathbb{P}[a_j = 1]$ ).

This correlation has a direct impact on the probability of collision of MinHash signatures. For example, if the hash signature contains  $k$  independent MinHash values of a fingerprint, and two of the non-zero elements responsible for the MinHash values are dependent, the hash signature has similar collision probability as the signature that contains only  $k - 1$  MinHash values. In other words, more fingerprints are likely to be hashed to the same bucket under this signature. For fingerprints shown in Figure 4, the largest 0.1% of the hash buckets contain an average of 32.9% of the total fingerprints for hash tables constructed with 6 hash functions.

**Performance impact of LSH parameters.** The precision and recall of the LSH is controlled via two key parameters: the number of hash functions  $k$  and the number of hash table matches

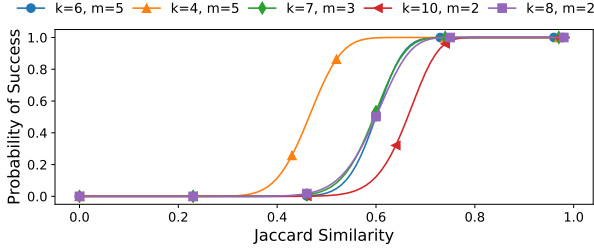


**Figure 5: Theoretical probability of a successful search versus Jaccard similarity between fingerprints ( $k$ : number of hash functions,  $m$ : number of matches). Different LSH parameter settings can have near identical detection probability with vastly different runtime.**

$m$ . Intuitively, using  $k$  hash functions is equivalent to requiring two fingerprints agree at  $k$  randomly selected non-zero positions. Therefore, the larger the number of hash functions, the lower the probability of collision. To improve recall, we increase the number of independent permutations to make sure that similar fingerprints can land in the same hash bucket with high probability.

Given two fingerprints with Jaccard similarity  $s$ , the probability that with  $k$  hash functions, the fingerprints are hashed to the same bucket at least  $m$  times out of  $t = 100$  hash tables is:

$$\mathbb{P}[s] = 1 - \sum_{i=1}^{m-1} \binom{t}{i} (1-s^k)^{t-i} (s^k)^i.$$

The probability of detection success as a function of Jaccard similarity has the form of an S-curve (Figure 5). If we increase the number of hash functions  $k$ , or the  $m$  threshold while keeping the other parameter fixed, the S-curve shifts to the right, increasing the Jaccard similarity threshold for LSH. Figure 5 illustrates a near-identical probability of success curve under different parameter settings.

Due to the presence of correlation in the input data, LSH parameters that result in the same success probability curve can have vastly different runtime in practice. As we increase the number of hash functions, the expected average size of hash buckets decreases. However, we find that, for seismic data, raising the number of hash functions can lead to an order of magnitude speedup in the similarity search. We investigate the impact of LSH parameters in Section 8.3.

One caveat of lowering the number of matches is that the probability of spurious matches increases. These spurious matches can be suppressed by scaling up the number of matches required and the number of total hash tables, at the cost of larger memory usage. We illustrate the empirical trade-off between the decrease in similarity search time and the increase in output size in Section 8.1.

## 6.4 Optimization: Partitioning

To further reduce the runtime as well as the memory footprint of the similarity search on large datasets, we found it necessary to perform the search in partitions and in parallel. We describe the details of each in this subsection.

**Partition.** Using a 1-second lag for adjacent fingerprints results in around 300M total fingerprints for 10 years of time series data.

Given a hash signature of 64 bits and 100 total hash tables, the total size of hash signature is approximately 250 GB. In addition, to avoid expensive disk I/O, we also need to keep all hash tables in memory for lookups. Taken together, this requires several hundred gigabytes of memory, which can exceed available main memory.

To support processing larger input data on a single node without modifying the semantics of the search, we perform the similarity search in partitions. Instead of initializing the hash tables with all fingerprints in the dataset, we partition the data and only insert fingerprints in the current partition to the hash tables. During lookup, we output matches between fingerprints in the hash table with all other fingerprints. We subsequently repeat this process for each partition. By partitioning the hashing, we only need to store a subset of the inputs in the hash tables in memory. In addition, if the hash signature table does not fit in memory, we can also partition the lookup tables. We illustrate the performance and memory trade-offs under different numbers of partitions in Section 8.3.

The partitioned search scheme is also useful when users are only performing similarity search for a limited number of queries (e.g., similarity with a fixed number of time segments). In this case, the cost of hash table initialization dominates that of the search, and it is often more efficient to initialize the hash tables with only the query fingerprints and query all other fingerprints against the small hash table. For example, initializing hash tables with 1M fingerprints and then performing 1000 queries can be 8.6× slower compared to initializing hash tables with the 1000 query fingerprints and performing 1M queries against the small tables.

We can further reduce the memory usage and increase the performance of LSH by implementing even more space efficient variants of LSH such as multi-probe LSH [42]. However, given that the alignment step of the pipeline uses the number of matches in the hash tables as the proxy for similarity, switching to a multiprobe implementation would change the semantics of the output, which we preserve for backwards compatibility with FAST. We demonstrate the potential benefits of implementing multi-probe LSH in Section 8.4.

**Parallelization.** The hash generation procedure can be easily parallelized once we have generated all the hash mappings: we divide the input fingerprints into partitions and calculate the signature for each partition in parallel.

Similarly, the query procedure can be parallelized by running nearest neighbor queries for different fingerprints in parallel. The only critical section in the search is on outputting nearest neighbors to file, which we optimize by writing to binary files. We show in Section 8.3 that the total hash signature generation time and similarity search time reduces linearly with the number of processes.

## 6.5 Optimization: Domain-specific filters

Like many other sensor measurements, seismometer readings can be noisy. In this subsection, we address a practical challenge of the detection pipeline, where similar non-seismic signals dominate seismic findings in runtime and detection results. We show that by leveraging domain knowledge, we can greatly increase both the efficiency and the quality of the detection.

**Filtering irrelevant frequencies.** Some input time series contain station-specific narrow-band noise that repeats over time. Patterns

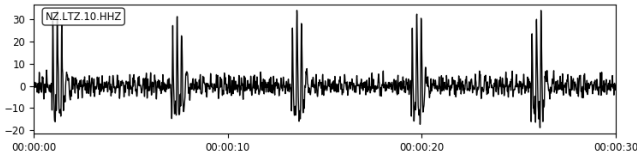


**Figure 6: The short, three-spike pattern is an example of similar and repeating background signals not due to seismic activity. These repeating noise patterns cause scalability challenges for LSH.**

of the repeating narrow-band noise are captured in the fingerprints and are identified as near neighbor, or earthquake candidates in the similarity search.

To address this problem, we apply a bandpass filter to exclude frequency bands that show high average amplitudes and repeating patterns while containing low seismic activities. The bandpass filter is selected manually by examining short spectrogram samples, typically an hour long, of the input time series, based on seismological knowledge, and typical bandpass filter ranges span from 2 to 20Hz. We investigate the impact of applying bandpass filters on both the runtime and result quality in the evaluation (Section 8.2).

**Removing correlated noise.** Repeating non-seismic signals can also occur in frequency bands containing rich earthquake signals. Figure 6 shows an example of strong repeating background signals from a New Zealand seismic station. A large cluster of repeating signals with high pairwise similarity could produce nearest neighbor matches that dominate the similarity search, leading to a  $10\times$  increase in runtime and an over  $100\times$  increase in output size compared to results from similar stations. This poses both problems for computational scalability and for seismological interpretability.

We develop an occurrence filter for the similarity search by exploiting the rarity of the earthquake signals. Specifically, if a specific fingerprint is generating many nearest neighbor matches during a short duration of time, we can be fairly confident that it is not an earthquake signal. This observation generally holds except for special scenarios such as volcanic earthquakes [11].

During the similarity search, we dynamically generate a list of fingerprints to exclude from future search. If the number of near neighbor candidates a fingerprint generates is larger than a predefined percentage of the total fingerprints, we exclude this fingerprint as well as its near neighbors from future similarity search. To capture repeating noise over a short duration of time, the filter can be applied on top of the partitioned search. In this case, the filtering threshold is defined as the percentage of fingerprints in the current partition, rather than of the whole dataset. On the example dataset above, this approach filtered out around 30% of the total fingerprints. We evaluate the effect of the occurrence filter on different datasets under different filtering thresholds in Section 8.2.

## 7 SPATIOTEMPORAL ALIGNMENT

The LSH-based similar search outputs pairs of similar fingerprints (or waveforms) from the input data, without knowledge of whether the pairs correspond to actual earthquake events. In this section, we show that by incorporating domain knowledge, we are able to

significantly reduce the size of the output and prioritize seismic findings in the similarity search results. We present aggregation and filtering techniques on the level of seismic channels, seismic stations and seismic networks (Section 7.1). We then describe the implementation challenges and our solutions to efficiently process large amounts of output (Section 7.2).

### 7.1 Alignment Overview

The similarity search outputs a list of similar binary fingerprint pairs that are candidates for reoccurring earthquakes with similar waveforms. The similarity search computes a sparse similarity matrix  $M$ , where the non-zero entry  $M[i, j]$  represents the similarity of fingerprints  $i$  and  $j$ . In order to identify weak events in low signal-to-noise ratio settings, seismologists set lenient detection thresholds for the similarity search. In practice, this means that the search often produces a large number of outputs. For example, one year of time series data can easily generate 100G of output, or more than 5 billion pairs of similar fingerprints. Since it is infeasible for seismologists to inspect all results manually, we want to automatically filter and align the similar fingerprint pairs into a list of potential earthquakes with high confidence.

Based on algorithms proposed in a recent work in seismology [13], we seek to reduce similarity search results at the level of seismic channels, stations and also across a seismic network. Figure 7 gives an overview of the spatiotemporal alignment procedure.

**Channel Level.** Most modern seismic stations have multicomponent accelerometers that measure ground movements at different orientations, which we refer to as channels. For example, a typical station has three channels, measuring movements at the vertical, North-South horizontal and East-West horizontal planes. Since channels at the same station experience movements simultaneously, we can directly merge detection results from each channel of the station by combining the corresponding similarity matrix. Given earthquake-triggered fingerprint matches tend to register at multiple channels whereas matches induced by local noise might only appear on one channel, we can prune detections by imposing a slightly higher similarity threshold on the combined similarity matrix. This is to make sure that we include either matches with high similarity, or weaker matches registered at multiple channels.

**Station Level.** For each combined similarity matrix, we want to cluster and summarize the nonzero entries of the matrix (or the fingerprint matches). Empirically, domain scientists have found that earthquake events can be characterized by a thin diagonal shape in the similarity matrix, which corresponds to a group of similar fingerprint pairs separated by a constant offset [13]. The constant offset represents the time difference, or the inter-event time, between a pair of reoccurring earthquake events. One pair of reoccurring earthquake events can generate a cluster of fingerprint matches in the similarity matrix, since event waveforms are longer than a fingerprint time window, and adjacent fingerprints have significant overlaps. Concretely, we group similar fingerprint pairs into clusters of thin diagonals and store a few summary statistics for each diagonal (e.g., the bounding box of the diagonal, the total number of similar pairs in the bounding box, and the sum of their similarity). Compared to storing every similar fingerprint pair, the clusters and summary statistics significantly reduce the output size.



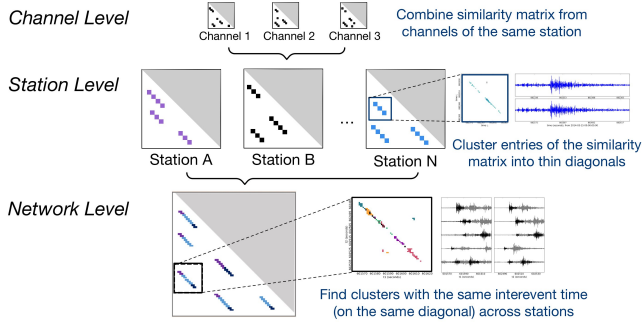


**Figure 7: The alignment procedure combines similarity search outputs from all channels in the same station (Channel Level), groups similar fingerprint matches generated from the same pair of reoccurring earthquakes (Station Level), and checks across seismic stations to reduce false positives in the final detection list (Network Level).**

**Network Level.** Earthquake signals also show strong temporal correlation across the seismic network, which we exploit to further suppress non-earthquake matches. Since an earthquake’s travel time is only a function of its distance from the source but not of the magnitude, reoccurring earthquakes generated from the same source take the same time to travel from the source to the seismic stations on each occurrence. Assume that an earthquake originated from source  $X$  takes  $\delta t_A$  and  $\delta t_B$  to travel to seismic stations  $A$  and  $B$  (Figure 8). Consider two occurrences of an earthquake from source  $X$  at time  $t_1$  and  $t_2$ . Station  $A$  experiences the arrivals of the two earthquakes at time  $t_1 + \delta t_A$  and  $t_2 + \delta t_A$ , while station  $B$  experiences the arrivals at  $t_1 + \delta t_B$  and  $t_2 + \delta t_B$ . The inter-event time  $\Delta t$  of these two earthquake events is independent of the location of the stations:

$$\Delta t = (t_2 + \delta t_A) - (t_1 + \delta t_A) = (t_2 + \delta t_B) - (t_1 + \delta t_B) = t_2 - t_1.$$

This means that in practice, diagonals with the same offset  $\Delta t$  and close starting times at multiple stations can be attributed to the same earthquake event. We require a pair of earthquake events to be observed at more than a user-specified number of stations in order to be considered as a detection.

On a run with 7 to 10 years of time series data from 11 seismic stations (27 channels), the postprocessing procedure effectively reduced the output from more than 2 Terabytes of similar fingerprint pairs to around 30K timestamps of potential earthquakes.

## 7.2 Implementation

The volume of similarity search output poses serious challenges for the alignment procedure, as we often need to process results larger than the main memory of a single node. In this subsection, we describe our implementation and out-of-core solutions.

**Similarity search output format.** The similarity search produces outputs that are in the form of triplets. A triplet  $(dt, idx1, sim)$  is a non-zero entry in the similarity matrix, which represents that fingerprint  $idx1$  and  $(idx1 + dt)$  are hashed into the same bucket  $sim$  times (out of  $t$  independent trials). We use  $sim$  as an approximation of the similarity between the two fingerprints.

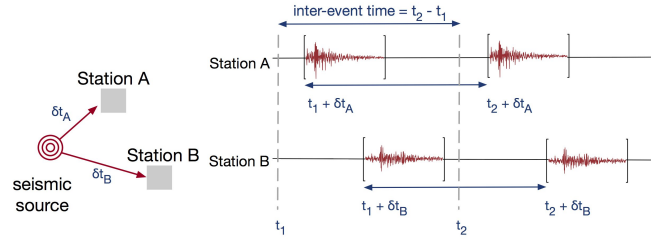


**Figure 8: Earthquakes from the same seismic sources has a fixed travel time to each seismic station (e.g.  $\delta t_A$ ,  $\delta t_B$  in the figure). The inter-event time between two occurrences of the same earthquake is invariant across seismic stations.**

**Channel.** First, given outputs of similar fingerprint pairs (or the non-zero entries of the similarity matrix) from different channels at the same station, we want to return the combined similarity matrix with only entries above a predefined threshold.

Naively, we could update a shared hashmap of the non-zero entries of the similarity matrix for each channel in the station. However, since the hashmap might not fit in the main memory on a single machine, we utilize the following sort-merge-reduce procedure instead:

- (1) In the sorting phase, we perform an external merge sort on the outputs from each channel, with  $dt$  as the primary sort key and  $idx1$  as the secondary sort key. That is, we sort the similar fingerprint pairs first by the diagonal that they belong to in the similarity matrix, and within the diagonals, by the start time of the pairs.
- (2) In the merging phase, we perform a similar external merge sort on the already sorted outputs from each channel. This is to make sure that all matches generated by the same pair of fingerprint  $idx1$  and  $idx1 + dt$  at different channels can be concentrated in consecutive rows of the merged file.
- (3) In the reduce phase, we traverse through the merged file and combine the similarity score of consecutive rows of the file that share the same  $dt$  and  $idx1$ . We discard results that have combined similarity smaller than the threshold.

**Station.** Given a combined similarity matrix for each seismic station, represented in the form of its non-zero entries sorted by their corresponding diagonals and starting time, we want to cluster fingerprint matches generated by potential earthquake events, or cluster non-zero entries along the narrow diagonals in the matrix.

We look for sequences of detections (non-zero entries) along each diagonal  $dt$ , where the largest gap between consecutive detections is smaller than a predefined gap parameter. Empirically, permitting a gap help ensure an earthquake’s P and S wave arrivals are assigned to the same cluster. Identification of the initial clusters along each diagonal  $dt$  requires a linear pass through the similarity matrix. We then interactively merge clusters in adjacent diagonals  $dt - 1$  and  $dt + 1$ , with the restriction that the final cluster has a relatively narrow width. To reduce the size of the total output, we only store a few summary statistics for each cluster, including a bounding box for the range of the cluster, number of non-zero entries in the cluster, the largest entry, and the sum of all entries in the cluster. We can

also eliminate isolated fingerprint pairs generated by background noise by applying a threshold on the clusters’ summary statistics.

The station level clustering dominates the runtime in the spatiotemporal alignment. In order to speed up the clustering, we partition the similarity matrix according to the diagonals, or ranges of  $dt$ s of the matched fingerprints. The above clustering procedure can then be performed in parallel on each partition.

**Network.** Given groups of potential events at each station, we perform a similar summarization across the network in order to identify subsets of the events that can be attributed to the same seismic source. We sort events at each station by the diagonal, or the inter-event time  $dt$ , and group events that share the same or adjacent diagonals and occur close in time. In principle, we could also partition and parallelize the network detection. In practice, however, we found that the summarized event information at each station is already small enough that it suffices to compute in serial.

## 8 EVALUATION

In this section, we perform both quantitative evaluation on performances of the detection pipeline, as well as qualitative analysis of the detection results. Our goal is to demonstrate that:

- (1) Each of our optimizations contributes to the performance improvement; together, our optimizations enable an over 100× speed up in the end-to-end detection pipeline.
- (2) Incorporating domain knowledge in the pipeline improves both the performance and the quality of the detection.
- (3) The improved scalability of the pipeline enables scientific discoveries on two public datasets: we discovered 597 new earthquakes from a decade of seismic data near the Diablo Canyon nuclear power plant in California and 6123 new earthquakes from a year of seismic data from New Zealand.

**Dataset.** We evaluate on two public datasets used in seismological analyses with our domain collaborators. The first dataset includes 1 year of 100Hz time series data (3.15 billion points per station) from 5 seismic stations (LTZ, MQZ, KHZ, THZ, OXZ) in New Zealand. We use the vertical channel (usually the least noisy) from each station [3]. The second dataset of interest includes 7 to 10 years of 100Hz time series data from 11 seismic stations and 27 total channels near the Diablo Canyon power plant in California [4].

**Experimental Setup.** We report results from evaluating the pipeline on a server with 512GB of RAM and two 28-thread Intel Xeon E5-2690 v4 2.6GHz CPUs. Our test server has L1, L2, L3 cache sizes of 32K, 256K and 35840K. We report the runtime averages from multiple trials.

### 8.1 End-to-end Evaluation

In this subsection, we report the runtime breakdown of the baseline implementation of the pipeline, as well as the effects of applying different optimizations.

To evaluate how our optimizations scale with data size, we evaluate the end-to-end pipeline on 1 month and 1 year of time series data from station LTZ in the New Zealand dataset. We applied a bandpass filter of 3-20Hz on the original time series to exclude noisy low-frequency bands. For fingerprinting, we used a sliding window with length of 30 seconds and slide of 2 seconds, which results in

Stages	Fingerprint	Hash Gen	Search	Alignment
Baseline	9.58	4.28	149	> 1 mo (est.)
+ freq filter	9.58	4.28	<b>30.9</b> (-79%)	<b>16.02</b>
+ #n func	9.58	<b>5.63</b> (+32%)	<b>3.35</b> (-89%)	<b>18.42</b> (+15%)
+ locality Min-Max	9.58	<b>1.58</b> (-72%)	3.35	18.42
+ MAD sample	<b>4.98</b> (-48%)	1.58	3.35	18.42
+ parallel (n=12)	<b>0.54</b> (-89%)	<b>0.14</b> (-91%)	<b>0.62</b> (-81%)	<b>2.25</b> (-88%)

**Table 1: Factor analysis (runtime in hours, and relative improvement) of each optimization on 1 year of time series data from station LTZ in New Zealand.**

1.28M binary fingerprints for 1 month of time series data (15.7M for one year), each of dimension 8192; for similarity search, we use 6 hash functions, and require a detection threshold of 5 matches out of 100 hash tables. We further investigate the effect of varying these parameters in the microbenchmarks in Section 8.3.

Figure 9 shows the cumulative runtime after applying each optimization. Cumulatively, our optimizations scale well with the size of the dataset, and enable an over 100× improvement in end-to-end processing time. We analyze each of these components in turn:

First, we apply a 1% occurrence filter (+ occur filter, Section 6.5) during similarity search to exclude frequent fingerprint matches generated by repeating background noise. This enables a 2-5× improvement in similarity search runtime while reducing the output size by 10-50×, reflected in the decrease in postprocessing time.

Second, we further reduce the search time by increasing the number of hash functions to 8 and lowering the detection threshold to 2 (+ increase #funcs, Section 6.3). While this increases the hash signature generation and output size, it enables around 10× improvement in search time for both datasets.

Third, we reduce the hash signature generation time by improving the cache locality and reducing the computation by with Min-Max hash instead of MinHash (+ locality MinMax, Section 6.2), which leads to a 3× speedup for both datasets.

Fourth, we speed up fingerprinting by 2× by enabling estimation of the MAD statistics with a 10% sample (+ MAD sample, Section 5.2).

Finally, we enable parallelism and run the pipeline with 12 processes (Section 5.2, 6.4, 7.2). As a result, we see an almost linear decrease in runtime in each part of the pipeline.

The improved scalability enables us to scale analytics from 3 month to over 10 years of data. We discuss qualitative detection results from both datasets in Section 8.5.

### 8.2 Effect of domain-specific optimizations

Here, we investigate the effect of applying domain-specific optimizations to the pipeline. We demonstrate that incorporating domain knowledge could improve both performance and result quality.

**Occurrence filter.** We evaluate the effect of applying the frequency based filter during similarity search on the five stations from the New Zealand dataset. The idea is to exploit the rarity of earthquakes events. Specifically, if a fingerprint is generating many matches in a short period of time during the similarity search, it is unlikely that the matches are due to real earthquake events. For this evaluation, we use a partition size of 1 month as the duration for

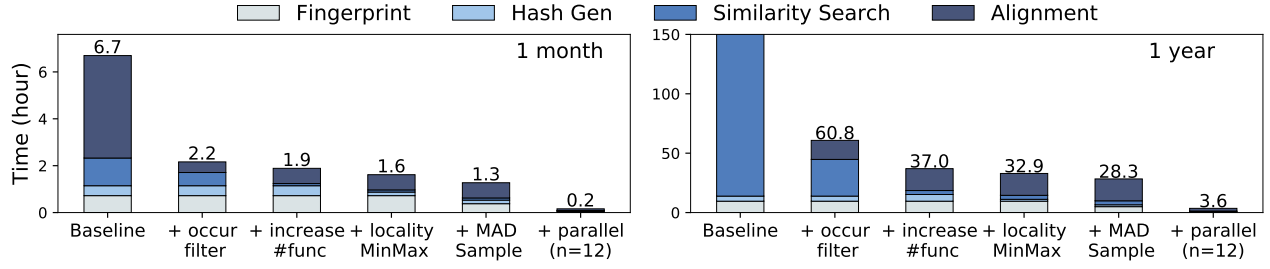


**Figure 9: Factor analysis of processing 1 month (left) and 1 year (right) of 100Hz data from LTZ station in the New Zealand dataset. We show that each of our optimization contributes to the performance improvements, and enabled an over 100 $\times$  speed up end-to-end.**

the frequency threshold; a 1% threshold indicates that a fingerprint matches over 10K other fingerprints in the same month.

We report the total percentage of fingerprints that are filtered under varying frequency thresholds in Table 2. We also evaluate the accuracy of the frequency filter by comparing the timestamps of filtered fingerprints with the catalog of the origin time of known earthquakes at each station. We report in Table 2 false positive rate, or the number of filtered earthquakes over the total number of cataloged events, of the filter under varying thresholds.

The results show that as the frequency threshold decrease, the percentage of filtered fingerprints and the false positive rate both increase. For seismic stations suffering from correlated noise, the frequency filter can effectively eliminate a significant amount of fingerprints from the similarity search. For station LTZ, a 1% frequency threshold filters out up to 30% of the total fingerprints without any false positives, which results in a 4 $\times$  improvement in runtime. For other stations, the frequency filter has little influence on the results. This is expected since these other stations do not have repeating noise signals such as those at station LTZ (Figure 6).

**Bandpass filter.** We compare similarity search on the same dataset before and after applying bandpass filters. The 100Hz sampling rate of the raw time series corresponds to a Nyquist frequency of 50Hz. The first bandpass filter (bp: 1-20Hz) is selected as most seismic signals are under 20Hz; the second (bp: 3-20Hz) is selected after manually looking at samples spectrograms of the dataset and excluding low frequencies that are noisy.

Figure 10 reports the similarity search runtime for fingerprints generated with different bandpass filters. Overall, similarity search suffers from additional matches generated from the noisy frequency bands outside the interests of seismology. For example, at station OXZ, removing the bandpass filter leads to a 16 $\times$  slow down in runtime and a 209 $\times$  increase in output size.

We compare detection recall on 8811 catalog earthquake events for different bandpass filters. The recall for the unfiltered data (0-50Hz), the 1-20Hz and 3-20Hz bandpass filters are 20.3%, 23.7%, 45.2%, respectively. Overall, by using a proper bandpass filter, we see an improvement in result quality, reflected in the increase in the number of detected catalog events. The overall low recall is expected, as we only used 4 (out of over 50) stations in the seismic network that contributes to the generation of catalog events.

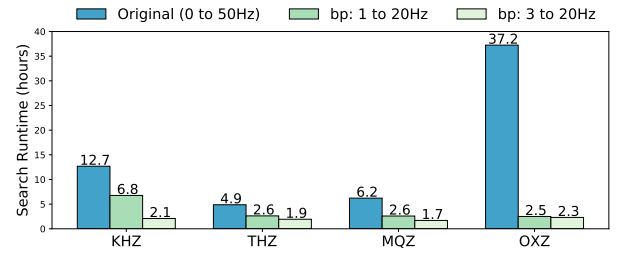


**Figure 10: LSH runtime under different band pass filters. Matches of noise in the non-seismic frequency bands lead to significant runtime increase for unfiltered time series.**

### 8.3 Effect of pipeline parameters

In this section, we evaluate the effect of the space/quality and time trade-offs for core pipeline parameters.

**MAD sampling rate.** We evaluate the speed and quality trade-off for calculating the median and MAD of the wavelet coefficients for fingerprints via sampling. We use the 1 month dataset in Section 8.1 (1.3M fingerprints) as input, and vary the sampling rate. In Table 3, we report the relative speed up in MAD calculation time as well as the average overlap between the binary fingerprints generated using the sampled MAD and the original MAD as a metric for accuracy.

The results illustrate that runtime reduces linearly with sampling rate, as expected. At lower rates, I/O begins to dominate MAD calculation runtime so the runtime improvements suffer from diminishing return. As a rule of thumb, we use the full dataset for MAD calculation for inputs shorter than a week, 1% or less sampling rate for inputs over a year and a 10% rate for inputs in between.

**LSH parameters.** We report runtime of the similarity search under different LSH parameters in Figure 11. As indicated in Figure 5, the three sets of parameters that we evaluate yield near identical probability of detection given Jaccard similarity of two fingerprints. However, by increasing the number of hash functions and thereby increasing the selectivity of hash signatures, we decrease the average number of lookups per query by over 10x. This results in around 10x improvement in similarity search time.

# Events	LTZ 1548			MQZ 1544			KHZ 1542			THZ 1352			OXZ 1248		
Filter Freq	FP	Filtered	Time	FP	Filtered	Time	FP	Filtered	Time	FP	Filtered	Time	FP	Filtered	Time
5.0%	0.00	0.88	149.3	0.00	0.00	2.8	0.00	0.00	2.2	0.00	0.00	2.4	0.00	0.00	2.6
1.0%	0.00	30.12	31.0	0.00	0.00	2.7	0.00	0.00	2.3	0.00	0.00	2.3	0.00	0.00	2.6
0.5%	0.00	31.19	32.1	0.00	0.09	2.8	0.00	0.00	2.4	0.00	0.00	2.4	0.08	0.08	2.7
0.1%	0.00	32.08	28.6	0.07	0.31	2.7	0.00	0.03	2.4	0.00	0.02	2.3	0.08	0.17	2.6

Table 2: The table shows that the percentage of fingerprints filtered (Filtered) and the false positive rate (FP) both increase with the decrease of filter frequency threshold. The runtime (in hours) measures similarity search time.

Sampling Rate	Average Fingerprint Overlap	Speedup
0.001	94.9%	350x
0.01	98.7%	99.8x
0.1	99.5%	10.5x
0.5	99.7%	2.2x
0.9	99.9%	1.1x

Table 3: Speedup and quality of different MAD sampling rate compared to no sampling on 1.3M fingerprints. Sampling enables a 100x speed up in MAD calculation while 98.7% accuracy. Below 1%, runtime improvements suffer from a diminishing return, as the IO begins to dominate the MAD calculation in runtime.

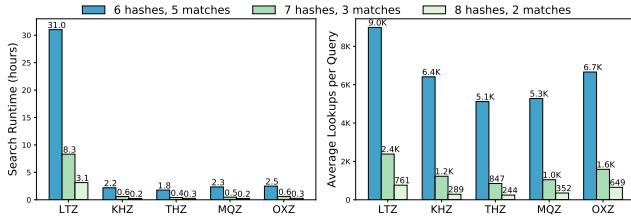


Figure 11: Effect of LSH parameters on similarity search runtime and average query lookups. Increasing the number of hash functions significantly decreases the query selectivity, which results in a 10 $\times$  improvement runtime.

**Number of partitions.** We report the runtime and memory usage of the similarity search with varying number of partitions in Figure 12. As the number of partitions increases, the runtime increases slightly due to the overhead of initialization and deletion of hash tables. In contrast, memory usage decreases as we only need to keep a subset of the hash signatures in the hash table at any time. Overall, by increasing the number of partitions from 1 to 8, we are able to decrease the memory usage by over 60% while incurring less than 20% runtime overhead. This allows us to run LSH on larger datasets with the same amount of memory.

**Parallelism.** Finally, to quantify the speedups from parallelism, we report the runtime of LSH hash signature generation and similarity search using a varying number of processes.

For hash signature generation, we report the hash mapping generation time as well as the Min-Max hash calculation time. For similarity search, we use the fixed hash signature as input for each station and vary the number of processes assigned during the search.

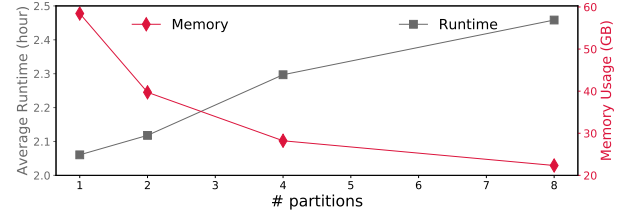


Figure 12: Runtime and memory usage for similarity search under a varying number of partitions. By increasing the number of search partitions, we are able to decrease the memory usage by over 60% while incurring less than 20% runtime overhead.

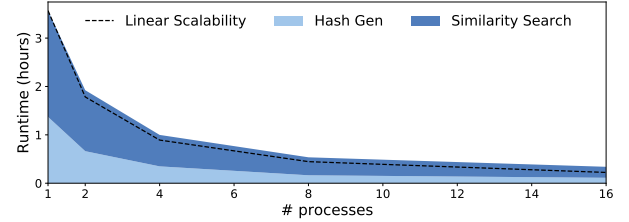


Figure 13: The plot shows a linear scalability for similarity search and hash signature generation.

We show the results in Figure 13. Overall, the total time for the hash signature generation and for the similarity search reduces near linearly with the number of processes.

## 8.4 Evaluation to Alternative Search Strategy

In this subsection, we compare the query performance of our similarity search to an alternative and more advanced open source LSH library. We were unable to find an existing high-performance implementation of LSH for Jaccard similarity, so we instead compare to FALCONN [1], a popular library based on recent theoretical advances in LSH family for cosine similarity [7].

We exclude hash table construction time, and compare single-core query time between FALCONN and our MinHash LSH. We use 74,795 input fingerprints with dimension 2048 and 10% non-zero entries. We tune both libraries such that for a small sample query set, the accuracy for finding the true nearest neighbor is at least 90%. With multi-probe LSH, FALCONN achieves an average query time of 0.68ms (16 hash functions, 50 hash tables and 400 probes); with “vanilla” (i.e., non-multiprobe) LSH, FALCONN achieves an



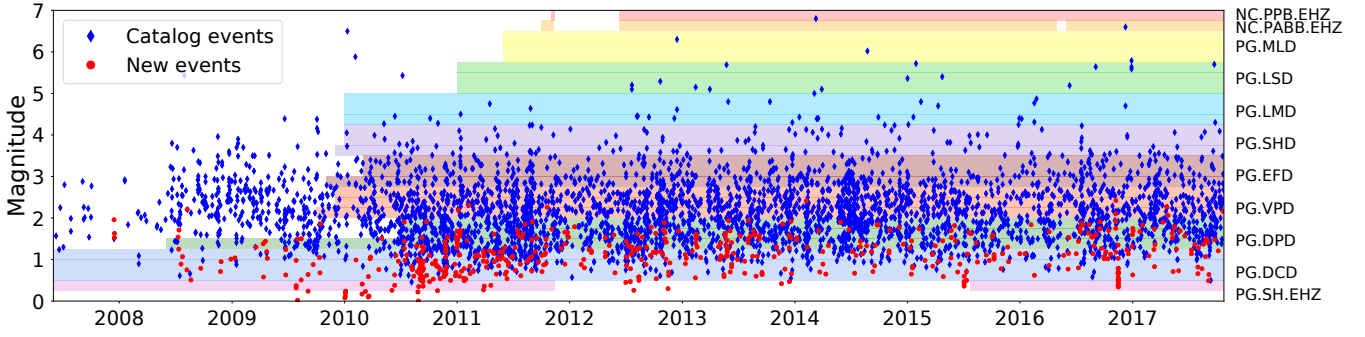


**Figure 14:** The left axis shows origin times and magnitude of detected earthquakes, with the catalog events marked in blue and new events marked in red. The colored bands in the right axis represent the duration of data used for detection collected from 11 seismic stations and 27 total channels. Overall, we detected 3957 catalog earthquakes (blue) as well as 597 new local earthquakes (red) from this dataset.

average query time of 2.68ms (16 hash functions, 200 hash tables). In comparison, our implementation has an average query time of 0.036ms (4 hash functions, 100 hash tables), which is 18.8 $\times$  and 74.4 $\times$  faster than FALCONN with multiprobe and vanilla LSH.

We suspect that the performance difference is a result of the mismatch between our binary input and FALCONN’s target similarity metrics. Our results are also consistent with previous findings that MinHash outperforms SimHash on binary, sparse input data [55].

## 8.5 Qualitative Results

We first report our findings in running the pipeline over a decade (06/2007 to 10/2017) of continuous seismic data from 11 seismic stations (27 total channels) near the Diablo Canyon nuclear power plant in central California. The chosen area is of special interest as there are many active faults near the power plant. Detecting additional small earthquakes in this region will allow seismologists to determine the size and shape of nearby fault structures, which can potentially inform seismic hazard estimates.

We applied station specific bandpass filters between 3 and 12 Hz to remove repeating background noise from the time series. Three stations also experienced corrupted data measurements, which we were able to filter out using occurrence filter during similarity search. The number of input binary fingerprints for each seismic channel ranges from 180 million to 337 million; the similarity search runtime ranges from 3 hours to 12 hours with 48 processes.

Among the 5048 detections above our detection threshold, 397 detections (about 8%) were false positives, confirmed via visual inspection: 30 were duplicate earthquakes with a lower similarity, 18 were catalog quarry blasts, 5 were deep teleseismic earthquakes (large earthquakes from >1000 km away). There were also 62 non-seismic signals detected across the seismic network; we suspect that some of these waveforms are sonic booms.

Overall, we were able to detect and locate 3957 catalog earthquakes, as well as 597 new local earthquakes. Figure 14 shows an overview of the origin time of detected earthquakes, which is spread over the entire ten-year span. The detected events include both low-magnitude events near the seismic stations, as well as larger events that are farther away. Figure 15 visualizes the locations of both catalog events and newly detected earthquakes, and Figure 16

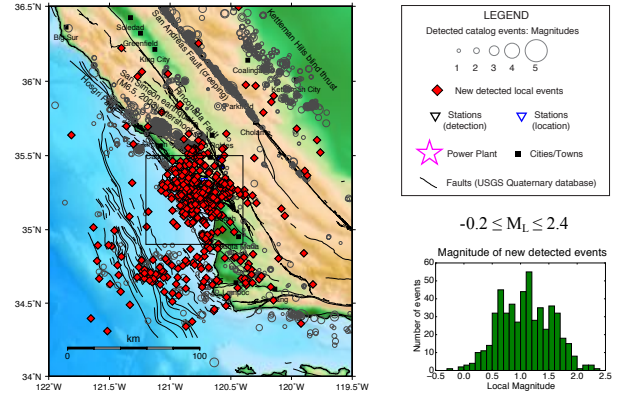


**Figure 15:** Overview of the location of detected catalog events (gray open circles) and new events (red diamonds). The pipeline was able to detect earthquakes close to the seismic network (boxed) as well as all over California.

zooms in on earthquakes in the vicinity of the power plant. Despite the low rate of local earthquake activity (535 total catalog events from 2007 to 2017 within the area shown in Figure 16), we were able to detect 355 new events that are between  $-0.2$  and  $2.4$  in magnitude and located within the seismic network, where many active faults exist. We missed 261 catalog events, almost all of which originated from outside the network of our interest. Running the detection pipeline at scale enables scientists to discover earthquakes from unknown sources. These new detections will be used to determine the details of active fault structures near the power plant.

We are also actively working with our domain collaborators on additional analysis of the New Zealand dataset. The pipeline detected 11419 events, including 4916 catalog events, 355 teleseismic events, 6123 new local earthquakes and 25 false positives (noise waveforms) verified by the seismologists. We are preparing these results for publication in seismological venues, and expect to further improve the detection results by scaling up the analysis to more seismic stations over a longer duration of time.

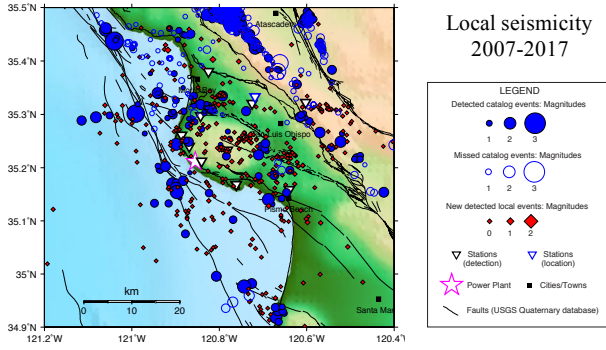


**Figure 16: Zoom in view of locations of new detected earthquakes (red diamonds) and cataloged events (blue circles) near the seismic network (box in Figure 15). The new local earthquakes contribute detailed information about the structure of faults.**

## 9 CONCLUSION

In this work, we reported on a novel application of LSH to large-scale seismological data, as well as the challenges and optimizations required to scale the system to over a decade of continuous sensor data. This experience in scaling LSH for large-scale earthquake detection illustrates both the potential and the challenge of applying core data analytics primitives to data-driven domain science on large datasets. On the one hand, LSH and, more generally, time series similarity search, is well-studied, with scores of algorithms for efficient implementation: by applying canonical MinHash-based LSH, our seismologist collaborators were able to meaningfully analyze more data than would have been feasible via manual inspection. On the other hand, the straightforward implementation of LSH in the original FAST detection pipeline failed to scale beyond a few months of data. The particulars of seismological data—such as frequency imbalance in the time series and repeated background noise—placed severe strain on an unmodified LSH implementation and on researchers attempting to understand the output. As a result, the seismological discoveries we have described in this paper would not have been possible without domain-specific optimizations to the detection pipeline. We believe that these results have important implications for researchers studying LSH (e.g., regarding the importance of skew resistance) and will continue to bear fruit as we scale the system to even more data and larger networks.

## REFERENCES

- [1] FALCONN - Fast Lookups of Cosine and Other Nearest Neighbors. <https://github.com/falconn-lib/falconn>.
- [2] FAST Detection Pipeline. <https://github.com/stanford-futuredata/quake>.
- [3] GeoNet. <https://www.geonet.org.nz/data/tools/FDSN>.
- [4] NCEDC. <http://service.ncedc.org/>.
- [5] SCEDC (2013): Southern California Earthquake Center. Caltech. Dataset. doi:10.7909/C3WD3xH1.
- [6] D. L. Anderson. *Theory of the Earth*. Blackwell scientific publications, 1989.
- [7] A. Andoni, P. Indyk, T. Laarhoven, I. Razenshteyn, and L. Schmidt. Practical and optimal lsh for angular distance. In C. Cortes, N. D. Lawrence, D. D. Lee, M. Sugiyama, and R. Garnett, editors, *Advances in Neural Information Processing Systems* 28, pages 1225–1233. Curran Associates, Inc., 2015.
- [8] W. Astuti, R. Akmeliawati, W. Sediono, and M. Salami. Hybrid technique using singular value decomposition (svd) and support vector machine (svm) approach for earthquake prediction. *IEEE Journal of Selected Topics in Applied Earth Observations and Remote Sensing*, 7(5):1719–1728, 2014.
- [9] S. Baluja and M. Covell. Audio fingerprinting: Combining computer vision & data stream processing. In *Acoustics, Speech and Signal Processing, 2007. ICASSP 2007. IEEE International Conference on*, volume 2, pages II–213. IEEE, 2007.
- [10] M. Bawa, T. Condie, and P. Ganesan. Lsh forest: self-tuning indexes for similarity search. In *Proceedings of the 14th international conference on World Wide Web*, pages 651–660. ACM, 2005.
- [11] A. F. Bell, S. Hernandez, H. E. Gaunt, P. Mothes, M. Ruiz, D. Sierra, and S. Aguiza. The rise and fall of periodic ãÿdrumbeatãÿ seismicity at tungurahua volcano, ecuador. *Earth and Planetary Science Letters*, 475:58 – 70, 2017.
- [12] K. Bergen, C. Yoon, and G. C. Beroza. *Scalable Similarity Search in Seismology: A New Approach to Large-Scale Earthquake Detection*, pages 301–308. Springer International Publishing, Cham, 2016.
- [13] K. J. Bergen and G. C. Beroza. Detecting earthquakes over a seismic network using single-station similarity measures. 2018. Manuscript submitted for publication.
- [14] D. Bobrov, I. Kitov, and L. Zerbo. Perspectives of cross-correlation in seismic monitoring at the international data centre. *Pure and Applied Geophysics*, 171(3):439–468, Mar 2014.
- [15] A. Broder. On the resemblance and containment of documents. In *Proceedings of the Compression and Complexity of Sequences 1997, SEQUENCES '97*, pages 21–, Washington, DC, USA, 1997. IEEE Computer Society.
- [16] J. Buhler. Efficient large-scale sequence comparison by locality-sensitive hashing. *Bioinformatics*, 17(5):419–428, 2001.
- [17] F.-P. Chan, A.-C. Fu, and C. Yu. Haar wavelets for efficient similarity search of time-series: with and without time warping. *IEEE Transactions on knowledge and data engineering*, 15(3):686–705, 2003.
- [18] O. Chum, J. Philbin, and A. Zisserman. Near Duplicate Image Detection: min-Hash and tf-idf Weighting.
- [19] G. Cortãs, F. Martãnez-ãlvarez, A. Morales-Esteban, J. Reyes, and A. Troncoso. Using principal component analysis to improve earthquake magnitude prediction in japan. *jzx049:1–14*, 10 2017.
- [20] H. Ding, G. Trajcevski, P. Scheuermann, X. Wang, and E. Keogh. Querying and mining of time series data: Experimental comparison of representations and distance measures. *Proc. VLDB Endow.*, 1(2):1542–1552, Aug. 2008.
- [21] W. Dong, Z. Wang, W. Josephson, M. Charikar, and K. Li. Modeling lsh for performance tuning. In *Proceedings of the 17th ACM Conference on Information and Knowledge Management, CIKM '08*, pages 669–678, New York, NY, USA, 2008. ACM.
- [22] C. E. Yoon, Y. Huang, W. L. Ellsworth, and G. C. Beroza. Seismicity during the initial stages of the guy-greenbrier, arkansas, earthquake sequence: Induced seismicity in guy, arkansas. 11 2017.
- [23] C. E. Yoon, O. O'Reilly, K. Bergen, and G. C. Beroza. Earthquake detection through computationally efficient similarity search. 1:e1501057–e1501057, 12 2015.
- [24] E. R. Engdahl, R. van der Hilst, and R. Buland. Global teleseismic earthquake relocation with improved travel times and procedures for depth determination. *Bulletin of the Seismological Society of America*, 88(3):722–743, 1998.
- [25] R. J. Geller and C. S. Mueller. Four similar earthquakes in central california. *Geophysical Research Letters*, 7(10):821–824, 1980.
- [26] S. J. Gibbons and F. Ringdal. The detection of low magnitude seismic events using array-based waveform correlation. *Geophysical Journal International*, 165(1):149–166, 2006.
- [27] A. Gionis, P. Indyk, and R. Motwani. Similarity search in high dimensions via hashing. In *Proceedings of the 25th International Conference on Very Large Data Bases, VLDB '99*, pages 518–529, San Francisco, CA, USA, 1999. Morgan Kaufmann Publishers Inc.
- [28] Y. J. Gu, A. Okeler, S. Contenti, K. Kocon, L. Shen, and K. Brzak. Broadband seismic array deployment and data analysis in alberta. *CSEG Recorder*, September, pages 37–44, 2009.
- [29] Y. Huang and G. C. Beroza. Temporal variation in the magnitude-frequency distribution during the guy-greenbrier earthquake sequence. *Geophysical Research Letters*, 42(16):6639–6646, 2015. 2015GL065170.
- [30] J. Ji, J. Li, S. Yan, Q. Tian, and B. Zhang. Min-max hash for jaccard similarity. In *2013 IEEE 13th International Conference on Data Mining*, pages 301–309, Dec 2013.
- [31] J. Johnson, M. Douze, and H. Jégou. Billion-scale similarity search with gpus. *arXiv preprint arXiv:1702.08734*, 2017.
- [32] M. Joswig. Pattern recognition for earthquake detection. *Bulletin of the Seismological Society of America*, 80(1):170, 1990.
- [33] B. Kang and K. Jung. Robust and efficient locality sensitive hashing for nearest neighbor search in large data sets. CiteSeer.
- [34] Z. Kang, W. T. Ooi, and Q. Sun. Hierarchical, non-uniform locality sensitive hashing and its application to video identification. In *2004 IEEE International Conference on Multimedia and Expo (ICME) (IEEE Cat. No.04TH8763)*, volume 1, pages 743–746 Vol.1, June 2004.
- [35] A. Kato and S. Nakagawa. Multiple slow-slip events during a foreshock sequence of the 2014 iquique, chile mw 8.1 earthquake. *Geophysical Research Letters*, 41(15):5420–5427, 2014. 2014GL061138.
- [36] E. Keogh and S. Kasetty. On the need for time series data mining benchmarks: a survey and empirical demonstration. *Data Mining and knowledge discovery*,

- 7(4):349–371, 2003.
- [37] Q. Kong, R. M. Allen, L. Schreier, and Y.-W. Kwon. Myshake: A smartphone seismic network for earthquake early warning and beyond. *Science Advances*, 2(2), 2016.
  - [38] B. Kulis and K. Grauman. Kernelized locality-sensitive hashing for scalable image search. In *2009 IEEE 12th International Conference on Computer Vision*, pages 2130–2137, Sept 2009.
  - [39] R. Kulkarni. A review of application of data mining in earthquake prediction. 01 2012.
  - [40] J. Leskovec, A. Rajaraman, and J. D. Ullman. *Mining of massive datasets*. Cambridge university press, 2014.
  - [41] T. W. Liao. Clustering of time series data—A survey. *Pattern recognition*, 38(11):1857–1874, 2005.
  - [42] Q. Lv, W. Josephson, Z. Wang, M. Charikar, and K. Li. Multi-probe lsh: efficient indexing for high-dimensional similarity search. In *Proceedings of the 33rd international conference on Very large data bases*, pages 950–961. VLDB Endowment, 2007.
  - [43] G. S. Manku, A. Jain, and A. Das Sarma. Detecting near-duplicates for web crawling. In *Proceedings of the 16th International Conference on World Wide Web*, WWW ’07, pages 141–150, New York, NY, USA, 2007. ACM.
  - [44] J. Peng, H. Wang, J. Li, and H. Gao. Set-based similarity search for time series. In *Proceedings of the 2016 International Conference on Management of Data*, pages 2039–2052. ACM, 2016.
  - [45] Z. Peng and P. Zhao. Migration of early aftershocks following the 2004 parkfield earthquake. *Nature Geoscience*, 2:877 EP –, 11 2009.
  - [46] T. Perol, M. Gharbi, and M. Denolle. Convolutional neural network for earthquake detection and location. *Science Advances*, 4(2), 2018.
  - [47] T. Rakthanmanon, B. Campana, A. Mueen, G. Batista, B. Westover, Q. Zhu, J. Zakaria, and E. Keogh. Searching and mining trillions of time series subsequences under dynamic time warping. In *Proceedings of the 18th ACM SIGKDD international conference on Knowledge discovery and data mining*, pages 262–270. ACM, 2012.
  - [48] B. Rao and E. Zhu. Searching web data using minhash lsh. In *Proceedings of the 2016 International Conference on Management of Data*, SIGMOD ’16, pages 2257–2258, New York, NY, USA, 2016. ACM.
  - [49] B. Rao and E. Zhu. Searching web data using minhash lsh. In *Proceedings of the 2016 International Conference on Management of Data*, pages 2257–2258. ACM, 2016.
  - [50] T. Sakaki, M. Okazaki, and Y. Matsuo. Earthquake shakes twitter users: real-time event detection by social sensors. In *Proceedings of the 19th international conference on World wide web*, pages 851–860. ACM, 2010.
  - [51] D. P. Schaff and G. C. Beroza. Coseismic and postseismic velocity changes measured by repeating earthquakes. *Journal of Geophysical Research: Solid Earth*, 109(B10):n/a–n/a, 2004. B10302.
  - [52] D. P. Schaff and F. Waldhauser. One magnitude unit reduction in detection threshold by cross correlation applied to parkfield (california) and china seismicity. 2010.
  - [53] D. R. Shelly, D. P. Hill, F. Massin, J. Farrell, R. B. Smith, and T. Taira. A fluid-driven earthquake swarm on the margin of the yellowstone caldera. *Journal of Geophysical Research: Solid Earth*, 118(9):4872–4886, 2013.
  - [54] W. Shi and B. M. G. Kibria. On some confidence intervals for estimating the mean of a skewed population. *International Journal of Mathematical Education in Science and Technology*, 38(3):412–421, 2007.
  - [55] A. Shrivastava and P. Li. In defense of minhash over simhash. In *Proceedings of the 17th International Conference on Artificial Intelligence and Statistics (AISTATS)*, volume 33, Reykjavik, Iceland, 2014.
  - [56] M. Vlachos, G. Kollios, and D. Gunopulos. Discovering similar multidimensional trajectories. In *Proceedings 18th International Conference on Data Engineering*, pages 673–684, 2002.
  - [57] J. Wang and T.-l. Teng. Identification and picking of s phase using an artificial neural network. *Bulletin of the Seismological Society of America*, 87(5):1140, 1997.
  - [58] Q. Wang, M. Cui, and H. Liang. Semantic-aware blocking for entity resolution. *IEEE Transactions on Knowledge and Data Engineering*, 28(1):166–180, Jan 2016.
  - [59] M. Withers, R. Aster, C. Young, J. Beiriger, M. Harris, S. Moore, and J. Trujillo. A comparison of select trigger algorithms for automated global seismic phase and event detection. *Bulletin of the Seismological Society of America*, 88(1):95, 1998.
  - [60] B.-K. Yi and C. Faloutsos. Fast time sequence indexing for arbitrary lp norms. In *Proceedings of the 26th International Conference on Very Large Data Bases*, VLDB ’00, pages 385–394, San Francisco, CA, USA, 2000. Morgan Kaufmann Publishers Inc.